Supporting Information for

Responsive Nanogel Probe for Ratiometric Fluorescent Sensing of pH and Strain in Hydrogels

Mingning Zhu[a], Dongdong Lu[a], Shanglin Wu[a], Qing Lian[a], Wenkai Wang[a], Amir H. Milani[a], Zhengxing Cui[a], Nam T. Nguyen[a], Mu Chen[a], L. Andrew Lyon[b], Daman J. Adlam[c], Anthony J. Freemont[c,d], Judith A. Hoyland[c,d] and Brian R. Saunders[a,*]

[a]*School of Materials, University of Manchester, MSS Tower, Manchester, M13 9PL, U.K.*

[b]*Schmid College of Science and Technology, Chapman University, Orange, CA, 92866, USA.*

[c]*Division of Cell Matrix Biology and Regenerative Medicine, Faculty of Biology, Medicine and Health, University of Manchester, Oxford Road, Manchester, M13 9PT, U.K.*

[d]*NIHR Manchester Musculoskeletal Biomedical Research Unit, Central Manchester Foundation Trust, Manchester Academic Health Science Centre, Manchester, UK.*

EXPERIMENTAL DETAILS

Materials

Methyl methacrylate (MMA, 99%), methacrylic acid (MAA, 99%), ethyleneglycol dimethacrylate (EGDMA, 98%), and glycidyl methacrylate (GMA, 97%), sodium dodecyl sulfate (SDS, 98.5%), ammonium persulfate (APS, 98%), chloroform ($CHCl_3$, 99%), phosphate buffered saline (PBS), NaOH (97%), *N*,*N*-dimethylformamide (DMF, 99%), $K_2S_2O_8$ (99%), acrylamide (AAm, 99%), Rhodamine B isothiocyanate (RBITC, 99%), potassium dihydrogen phosphate (PDP, 98%) *N*,*N*-Methylenebis(acrylamide) (MBAAm, 99%) and *N,N,N',N'*-tetramethylethylenediamine (TEMED, 99%) were all purchased from Sigma-Aldrich and used as received. (9-Phenanthryl)methylmethacrylate (Ph) and (9-anthryl)methacrylate (An) were obtained from Carbosynth Limited. Laponite RD (LAP) was obtained from Rockwood Limited. All chemicals were used as received. The water used was doubly filtered and deionized.

Vinyl-functionalized nanogel synthesis

The precursor (non-vinyl functionalized) nanogel preparation was performed using emulsion polymerization (Scheme S1a). SDS (2.4 g) in water (480 g) was added to a three-neck round flask equipped with a mechanical stirrer and reflux condenser. The contents were de-oxygenated and purged with nitrogen for at least 30 min. The co-monomer solution (106 g) used to prepare the NG contained MMA (79.2 wt.%), MAA (18.9 wt.%), EGDMA (1.9 wt.%). Emulsion polymerization was commenced by increasing the temperature to 80 ^{o}C and then aqueous APS (4.0 g of solution with a concentration of 7.9 wt. %) was quickly added and the reaction continued for 4 h. All NG dispersions were purified via extensive dialysis (14 kDa MWCO, Fisher Scientific).

The precursor nanogel particles were vinyl-functionalized using GMA via an epoxide ring-opening reaction following earlier work[1]. The vinyl-functionalized nanogel particles are referred to as NG. (See Scheme S1a) Briefly, the precursor nanogel dispersion (12 g, 5 wt.%) was reacted with GMA

(0.426 g, 3.0 mmol). The pH was adjusted to 5.1 and the dispersion heated at 40 ^{o}C for 8 h. The NG particles were washed extensively with $CHCl_3$ and residual solvent removed by rotary evaporation.

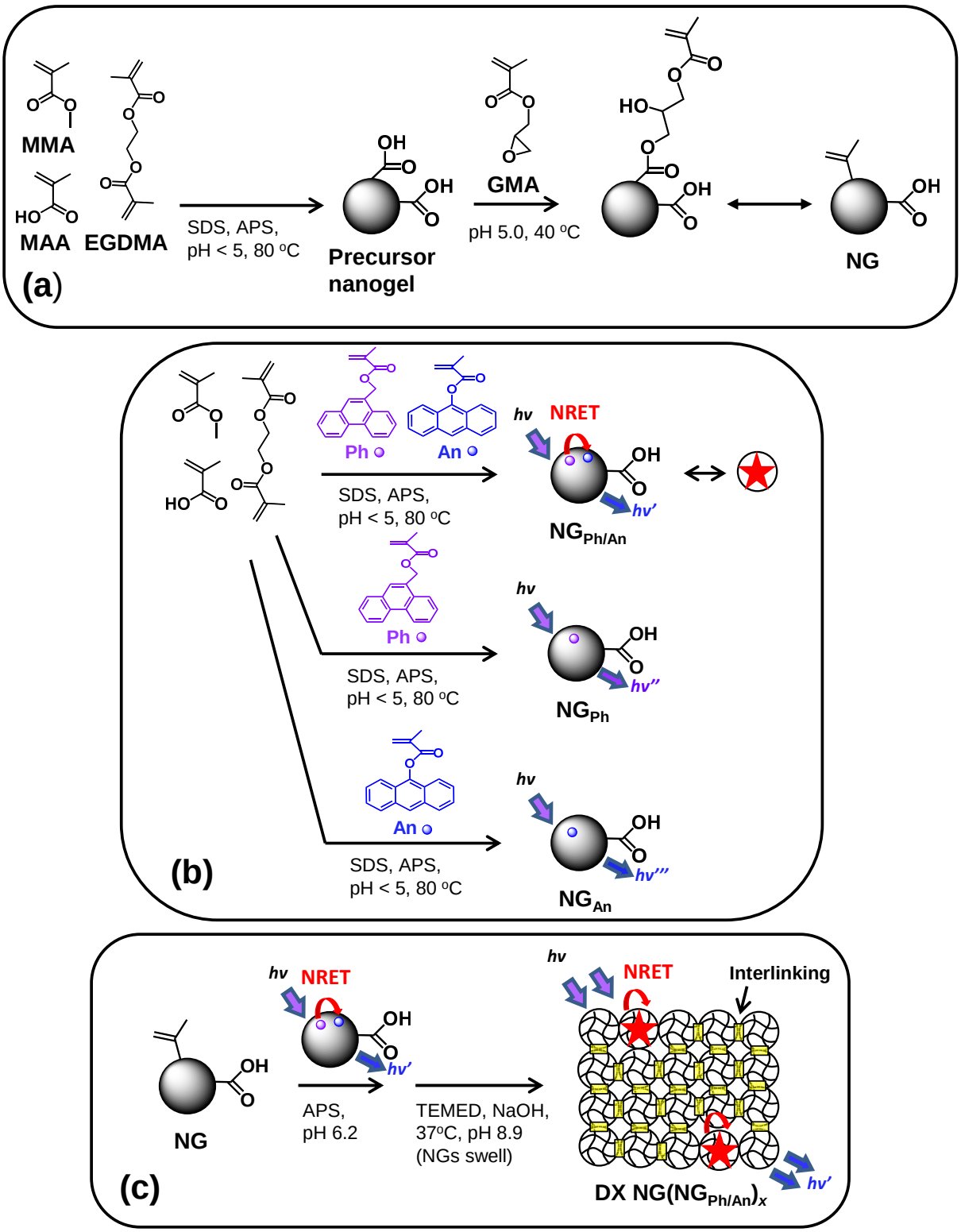

Scheme S1. (a) Depiction of the synthesis of precursor poly(MMA-MAA-EGDMA) nanogels and vinyl-functionalized nanogels (NG). (b) Synthesis of nanogels containing An and Ph ($NG_{An/Ph}$), Ph (NG_{Ph}) and An (NG_{An}). (c) Synthesis of DX NG($NG_{An/Ph}$)$_x$ gel where x is the wt% of $NG_{Ph/An}$ used.

Synthesis of fluorescently-labelled nanogel particles

The method used to prepare the fluorescently labelled nanogels is based on earlier work using temperature-responsive microgels[2] and is depicted in Scheme S1b. These nanogels were *not* vinyl-functionalized. The same general procedure as outlined above to prepare the precursor nanogel particles was used but with a smaller scale. Nanogels labelled with only Ph (NG_{Ph}) or An (NG_{An}) were prepared as controls in addition to the nanogel probe particles which contained both Ph and An ($NG_{Ph/An}$). NG_{Ph} and NG_{An} contained a nominal Ph or An concentrations of 0.50 mol%. The $NG_{Ph/An}$ particles were prepared using 0.25 mol% of Ph and An with respect to monomer. Table S1 shows the quantities used. Ph or An (or both) were dissolved in the co-monomer solution and then fed into the 100 mL three-neck flask which was stirred magnetically with nitrogen bubbling for at least 30 min and initiator was added to begin emulsion polymerization. The reaction was allowed to proceed for 4 h. To remove free fluorophore the nanogels were dialyzed against water/DMF (volume ratio: 80/20) for 7 days and then pure water for an additional 14 days. Characterization data for the various nanogels are shown in Table S2 and discussed below.

Synthesis of doubly crosslinked nanogels containing nanogel probe particles

Four double crosslinking nanogel DX NG($NG_{Ph/An}$)$_x$ (x = 0.02, 0.10 or 0.50) gels containing NG 10.8 wt.% and 0.02, 0.10 or 0.50 wt.% $NG_{Ph/An}$ with respect to the total gel mass were prepared (See Scheme S1c). A combined mixed dispersion was first prepared that comprised two pre-cursor mixtures (A and B). DX NG($NG_{Ph/An}$)$_x$ (x = 0.02, 0.10 and 0.50) gels were prepared using Mixture A which contained APS (52 μL of 0.156 mol/L solution), NG (2.166 g, 19.4 wt.%), and $NG_{Ph/An}$ (0.053 g, 0.267 g or 1.334 g for x = 0.02, 0.10 and 0.50, respectively, with a concentration of 1.31 wt.%) at a pH of 6.2. Mixture B comprised 0.350 g taken from a stock solution prepared using NaOH (9400 μL, 4.0 M), alkaline TEMED (300 μL), and water (300 μL) for DX NG($NG_{Ph/An}$)$_{0.50}$. In the cases where x = 0.10 or 0.02 another 1.067 or 1.280 g respectively of water was added to Mixture B. The final pH of the combined mixed dispersion was 8.9. The latter was transferred to a

rubber O-ring (outer diameter = 15 mm and thickness = 1 mm) and secured between two glass slides and cured at 37 ºC for at least 2 h.

Synthesis of poly(acrylamide) gel containing nanogel probe particles

The following is based on a literature method[3] which was modified to prepare poly(acrylamide) (PAAm-MBAAm) gel containing 0.10 wt.% nanogel probes (i.e. PAAm-MBAAm($NG_{Ph/An}$)$_{0.10}$). Briefly, AAm (188 mg, 2.64 mmol), MBAAm (5.0 mg, 32.5 μmol), water (2.0 g) were added to an aqueous dispersion (0.640 mL) containing fluorescent $NG_{Ph/An}$ (3.2 mg) for 10 min. APS (1.0 ml of 21.9 mmol/L solution) was added to the mixed dispersion under N_2 and stirred for 3 min and the solution (pH 5.6) transferred to a rubber O-ring (outer diameter = 13 mm and thickness = 1.8 mm) and cured at 50 ^{o}C for 5 h.

Synthesis of nanocomposite gel containing nanogel probe particles

An earlier synthetic method used to prepare nanocomposite gels was modified for use in this study[4]. LAP dispersion (2.06 wt%) was prepared by dispersing LAP powder thoroughly in deionized water (9.70 mL) under magnetic stirring for at least 2 h. AAm (1.0 g, 14 mmol), $NG_{Ph/An}$ (0.78 g of 0.49 wt.% dispersion), TEMED (10.0 μL) and $K_2S_2O_8$ (0.010 g, 0.040 mmol) were added, respectively, to the dispersion and mixed thoroughly. Curing was conducted at room temperature for at least 20 h. The final gel was formed in a cylinder mold with dimensions (height = 12 mm and diameter = 12 mm). The final pH was 10.7.

Physical Measurements

Potentiometric titration data were obtained using aqueous NaCl (0.01 M) with a Mettler Toledo titrator. Dynamic light scattering (DLS) and electrophoretic mobility data were obtained using a Malvern Zetasizer Nano-2S instrument. TEM observations were conducted using a Philips CM 20, and the samples were negatively stained using phosphotungstic acid (1.0 wt% aqueous solution). A Hitachi U-1800 spectrophotometer was used for UV-visible spectroscopy measurements. The photoluminescence (PL) spectra and absolute fluorescence quantum yield were obtained using an

Edinburgh Instruments FLS980 spectrometer. The excitation wavelength was 298 nm and the number of repeat measurements was five. This wavelength was also used to obtain the fluorescent images of the gels.

The absolute quantum yield was determined using PL over a range of emission wavelengths (320 to 600 nm) and measurements performed in a quartz sample holder using an integrating sphere. The overall quantum yield (Φ_{overall}) was calculated using[5]

$$\Phi_{\text{overall}} = \frac{\text{S(Em)}}{\text{S(Abs)}} = \frac{\int \frac{\lambda}{hc}[I_{\text{sample(em)}}(\lambda) - \text{I}_{\text{reference(em)}}(\lambda)]\text{d}\lambda}{\int \frac{\lambda}{hc}[\text{I}_{\text{reference(ex)}}(\lambda) - \text{I}_{\text{sample(ex)}}(\lambda)]\text{d}\lambda} \qquad \text{(S1)}$$

where *S(Abs)* is the number of photons absorbed by the sample and *S(Em)* is the number of photons emitted from the sample, λ is the wavelength, h is Planck's constant, c is the velocity of light, $I_{sample(ex)}$ and $I_{reference(ex)}$ are the integrated intensities of the excitation beam with and without the sample, and $I_{sample(em)}$ and $I_{reference(em)}$ are the PL intensities with and without the sample, respectively.

The volume swelling ratio (Q) of gels was measured using a gravimetric method. Samples were placed in phosphate buffer solutions (0.1 M) at different pH values. Each sample was weighed once a day and returned to a fresh buffer solution. The Q value for the gels was calculated using:

$$Q = \rho_{\text{p}}\left(\frac{Q_{(m)}}{\rho_{\text{s}}} + \frac{1}{\rho_{\text{p}}}\right) - \frac{\rho_{\text{p}}}{\rho_{\text{s}}} \qquad \text{(S2)}$$

where $Q_{(m)}$ is the mass swelling ratio. The ρ_s and ρ_p are the densities of the solvent (water) and polymer, respectively. The values used for water and the DX NGs were 1.0 and 1.2 g/mL, respectively. The ρ_p value for PAAm used was 1.30 g/mL[6]. In this study we use the average linear swelling ratio ($\alpha = Q^{1/3}$) to characterize gel swelling. Uniaxial compression tests were conducted using an Instron series 5569 load frame equipped with a 10 N compression testing head. Engineering stress and strain values are reported. A cylindrical geometry was used for the samples (diameter of 12 mm and height of 12 mm). PL spectra for gels being uniaxially compressed were obtained using a home-constructed optical-compression device which contained the gel between

two quartz slides with a known separation that could be varied. The device was placed within the FLS980 during measurements. The variation of the gel thickness enabled calculation of the engineering strain. The dimensions of the samples were the same as that used for uniaxial compression (above).

Reversibility studies for nanogel probes in dispersion or within DX NGs

The $NG_{Ph/An}$ dispersion (0.03 wt.%) in PDP buffer (pH 6.0) was placed in dialysis tubing (68 kD MWCO, Fisher Scientific) and this was placed in a much greater volume of buffer solution which was periodically switched from pH 6.0 to 8.0. A period of 24 h was allowed for the internal pH to equilibrate at the new pH value. A similar process was used for DX NG$(NG_{Ph/An})_{0.10}$ gel; however, dialysis tubing was not used.

Studying the effect of Ca^{2+} using nanogel probes in dispersion or within a DX NG

The pH of the $NG_{Ph/An}$ dispersion was adjusted to 9.0 by addition of aqueous NaOH (0.5 M) and the dispersion was investigated using DLS and PL after aqueous $CaCl_2$ solution was added (with mixing) to give 0.02 M increments. For the DX NG/$(NG_{Ph/An})_{0.10}$ gel, PL spectra were obtained using 0.02 M increments in aqueous $CaCl_2$ solutions with an equilibration time of 24 h for each concentration.

Release experiments for DX NG($NG_{Ph/An}$) gel containing RBITC

The RBITC-based fluorescent DX NG/$(NG_{Ph/An})_{0.10}$ gel was prepared using a modification of the procedure described above. In this case RBITC (0.14 wt.%, 20 μL) was added to Mixture A where the latter contained NG (3.095 g of 19.43 wt.% dispersion), $NG_{Ph/An}$ (0.381 g of 1.31wt.% dispersion) and APS (0.156 mol/L, 74 μL). Mixture B (0.55 mL) contained TEMED (300 μL), NaOH (9.4 mL of 4.0 M solution) and water (300 μL). The gel was cured as described above. Triggered release was performed by placing samples in PDP buffer for 24 h with different pH values. To quantify the amount of RBITC released from gel the Beer–Lambert law and a calibration curve was used (See Figure S16a).

Cytotoxicity studies

Human nucleus pulposus (NP) cells were cultured in Dulbecco's modified Eagle's medium supplemented with 10% fetal bovine serum (FBS, Gibco) and antibiotic/antimycotic (Sigma-Aldrich, UK) at 37 °C in a humidified 5% CO_2 atmosphere. Cells were seeded at a density of 3 x 10^4 per well onto 13 mm sterile glass coverslips in 24 well cell culture plates and allowed to attach overnight. For studies using the nanogel probes, $NG_{Ph/An}$ was added to wells to achieve a final concentration of 10^{-3} wt.%. In the case of the DX NG/$(NG_{Ph/An})_{0.10}$ gel, toroids were sterilized in 70% ethanol, then washed in sterile phosphate buffered saline (PBS) before being introduced into the culture wells (n = 3 per time-point). Control wells received an equal volume of PBS. Cell viability was determined at the appropriate time-points by live/dead assay (Life Technologies, UK). Controls with dead cells were prepared by fixing cells with methanol. Cells exposed to $NG_{Ph/An}$ were also fixed with 4% paraformaldehyde and mounted with Prolong Gold antifade (Life technologies, UK) +/- DAPI nuclear stain. Images were taken with an Olympus BX51 fluorescence microscope and a Lietz Diavert inverted light microscope.

SUPPLEMENTARY DISCUSSION AND FIGURES

Nanogel probe characterization

Four nanogel systems were prepared in this study: NG, NG_{Ph}, NG_{An} and $NG_{Ph/An}$. Synthesis details are given above and in Table S1. Only the NG particles were vinyl-functionalized. $NG_{Ph/An}$, NG_{Ph} and NG_{An} were fluorescently labelled and were *not* vinyl functionalized. (NG_{Ph} and NG_{An} were control systems.) Characterization data for all the nanogels are shown in Table S2. The collapsed particle sizes for $NG_{Ph/An}$ and NG were in the range of 16 - 17 nm as determined by TEM (Figure S3). The z-average diameters (d_z) values at pH 4.5 (collapsed state) were in the range 24 – 30 nm and were larger than the respective number-average diameters determined by TEM. This result was due to the strong dependence of d_z values on scattering from the largest particles. The scattered intensity ~ sixth power of particle size[7]. The apparent pK_a and MAA content for the $NG_{Ph/An}$ particles determined from potentiometric titration data (Figure S1) were 7.7 and 20.4 mol%, respectively. (The apparent pK_a is the pH corresponding to 50% neutralization.) DLS data are shown for the NG, NG_{Ph} and NG_{An} dispersions in Fig S4; whilst, DLS data for $NG_{Ph/An}$ are shown in Figure 1a. The nanogel d_z values increased when the pH increased to 5.4 and above. Variable pH electrophoretic mobility data for the $NG_{Ph/An}$ particles were measured (Figure S5) and became increasingly negative as the pH increased. This result was due to the particles becoming increasingly negatively charged as –COOH groups were ionized to $-COO^-$.

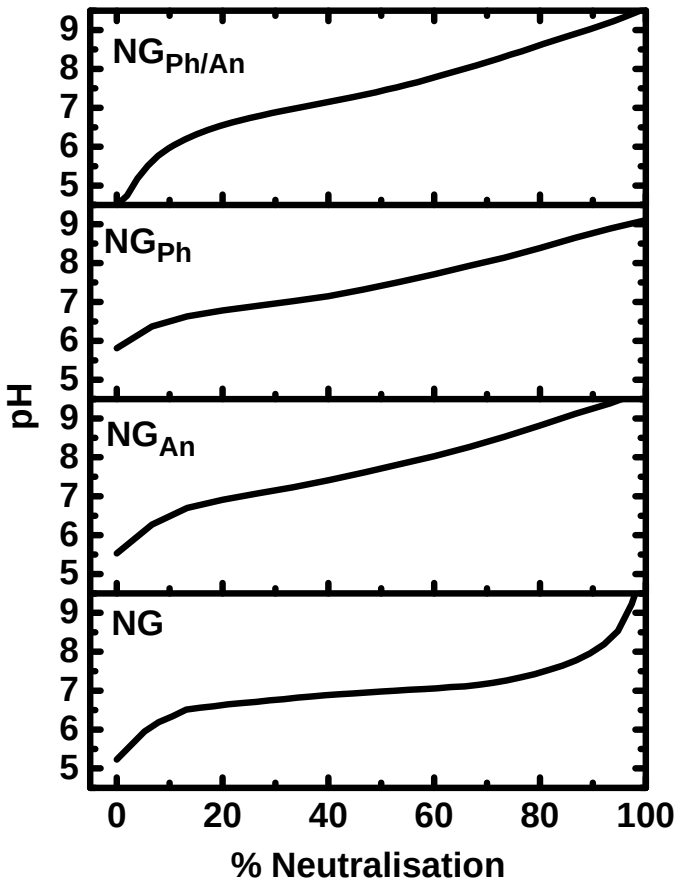

Figure S1. Potentiometric titration data for $NG_{Ph/An}$, NG_{Ph}, NG_{An} and NG dispersions.

Determining Ph and An contents for the $NG_{Ph/An}$, NG_{Ph} and NG_{An} particles

UV-visible spectroscopy was used to determine the Ph and An contents in the $NG_{Ph/An}$, NG_{Ph} and NG_{An} particles. The calibration graphs for the dyes (Figure S2) allowed the Ph and An contents in the nanogels to be determined using the Beer-Lambert law. UV-vis spectra for $NG_{Ph/An}$ (Figure S6a) showed that both dyes had been successfully incorporated. The particles contained 0.42 and 0.59 mol%, respectively, of Ph and An (Table S2). UV-visible spectra for NG_{Ph} and NG_{An} are shown in Figure S6b and S6c, respectively.

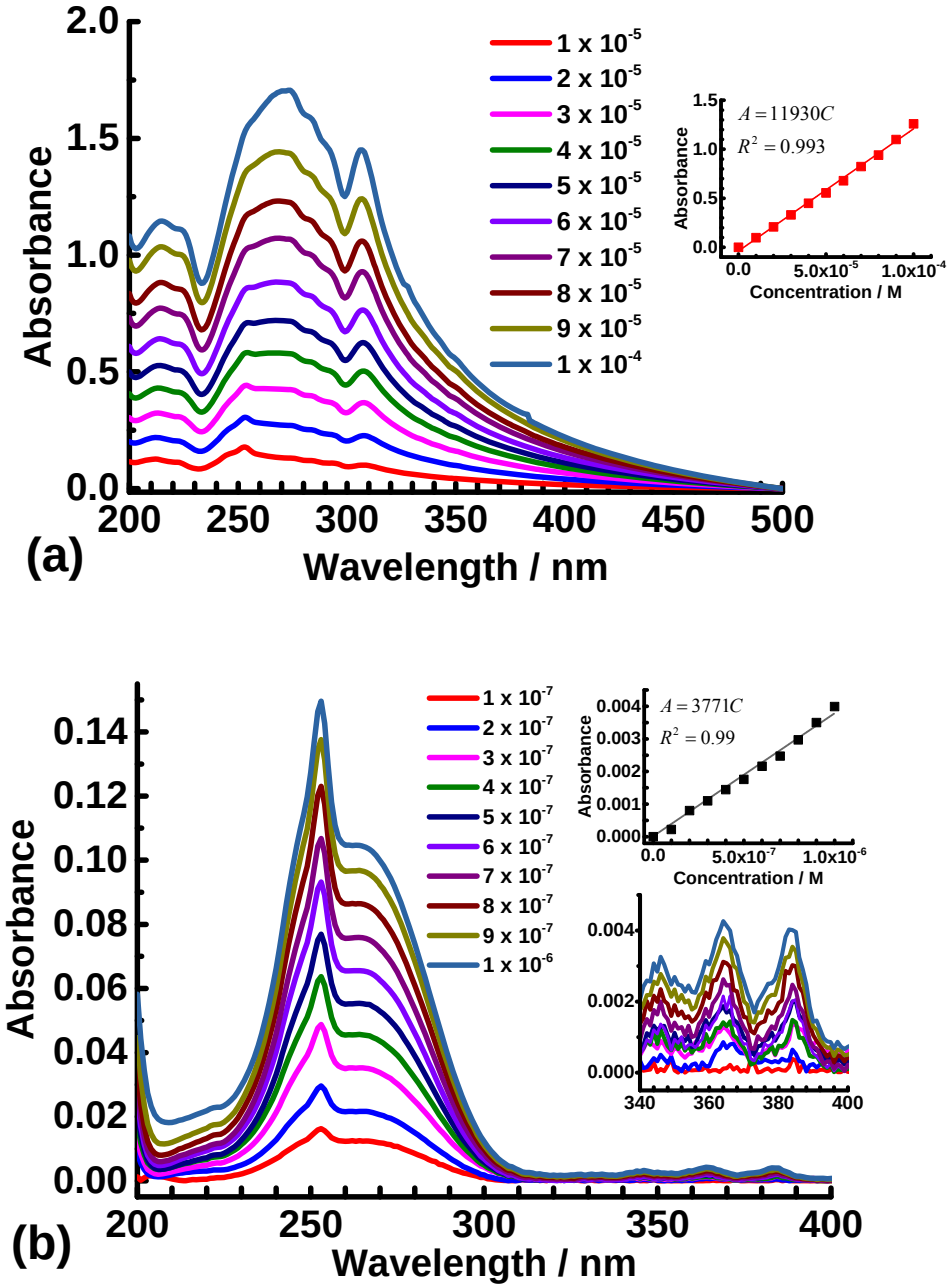

Figure S2. UV-visible spectra and calibration curves used for (a) Ph and (b) An dissolved in water. The concentrations are shown in the legends (M). The insets show the absorbance values at (a) 298 and (b) 366 nm as a function of fluorophore concentration.

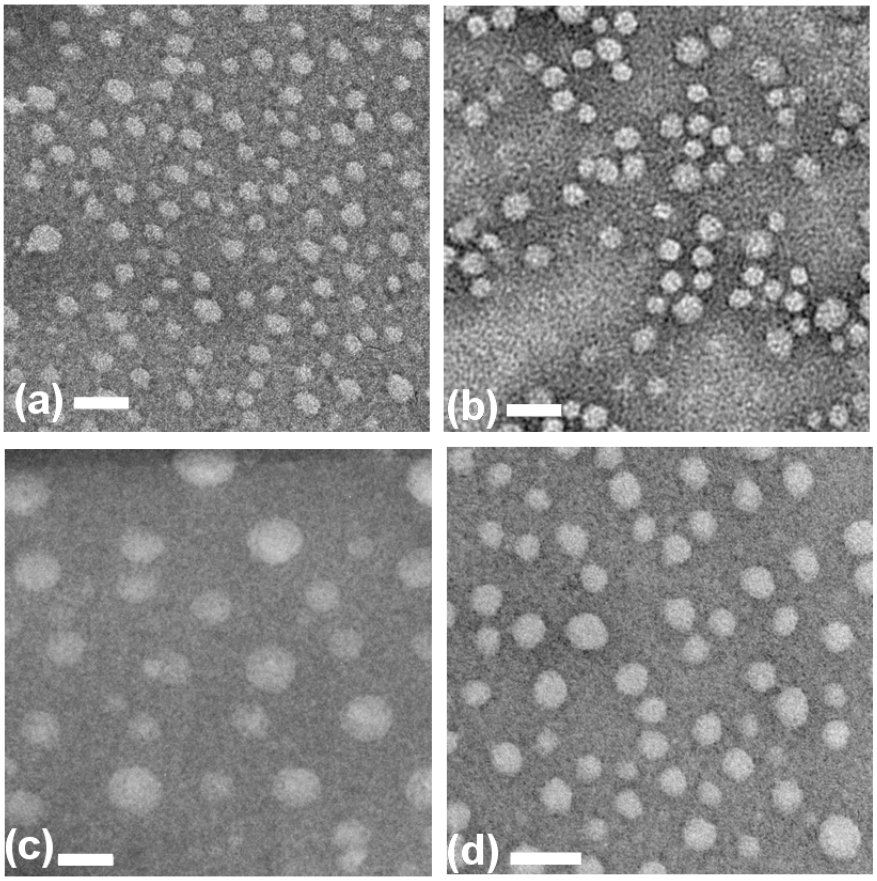

Figure S3. Representative TEM images for (a) $NG_{Ph/An}$, (b) NG as well as control (c) NG_{Ph} and (d) NG_{An} particles. The scale bars are 50 nm.

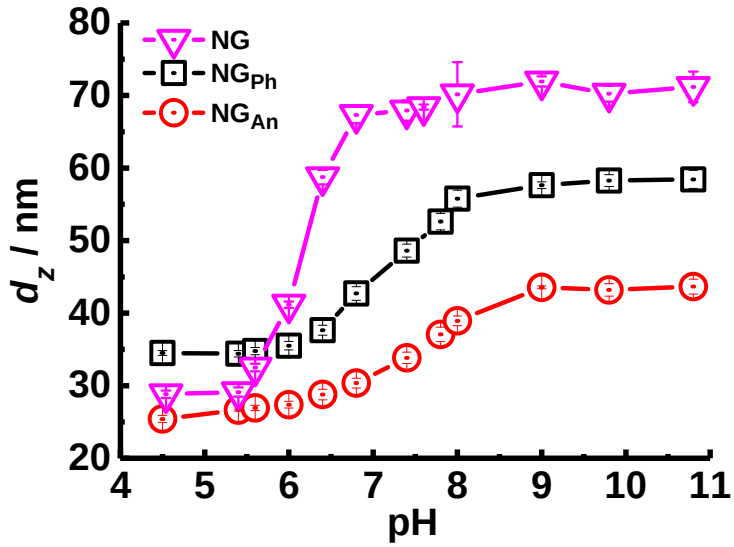

Figure S4 DLS data as a function of pH for NG, NG_{Ph} and NG_{An} dispersions.

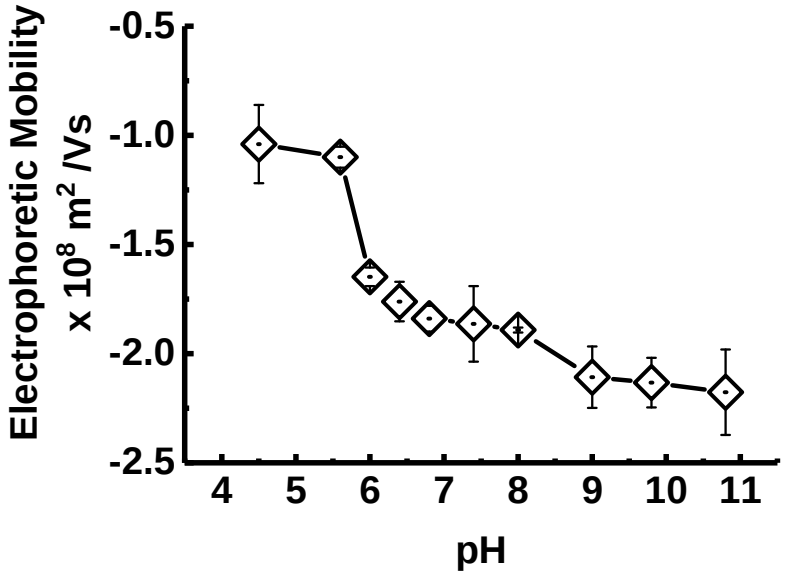

Figure S5 Electrophoretic mobility as a function of pH for dispersed $NG_{Ph/An}$.

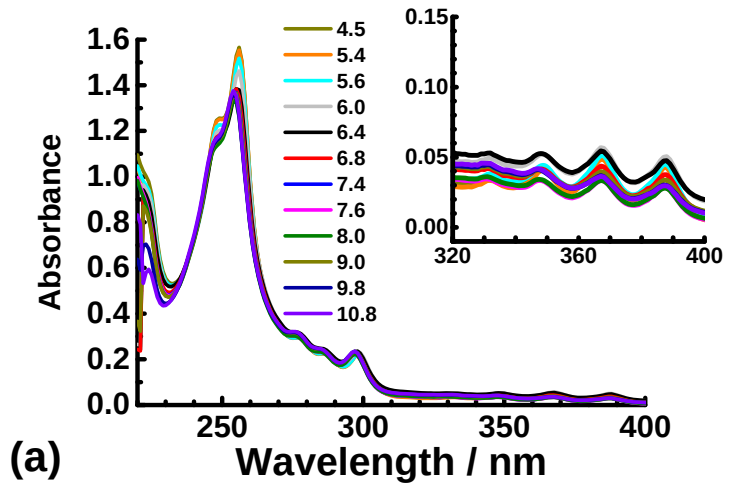

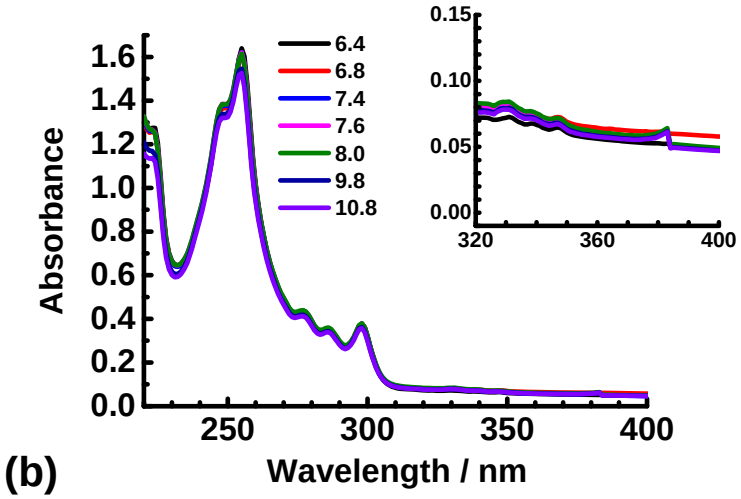

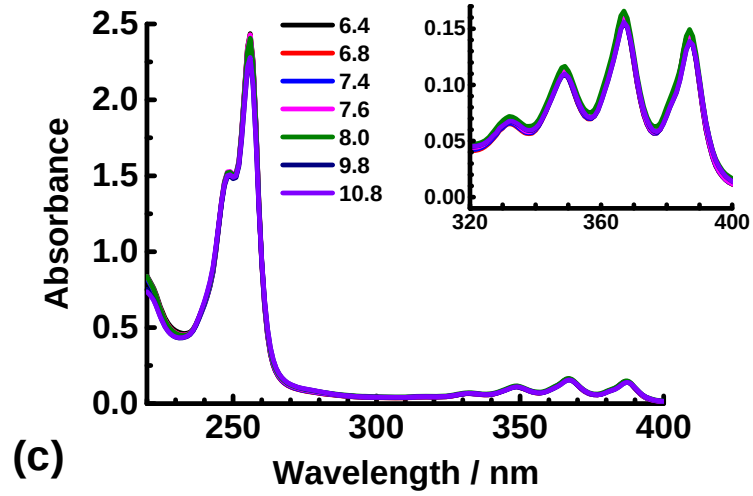

Figure S6 UV-visible spectra for (a) $NG_{Ph/An}$, (b) NG_{Ph} and (c) NG_{An} dispersions. The insets show expanded views of the spectra.

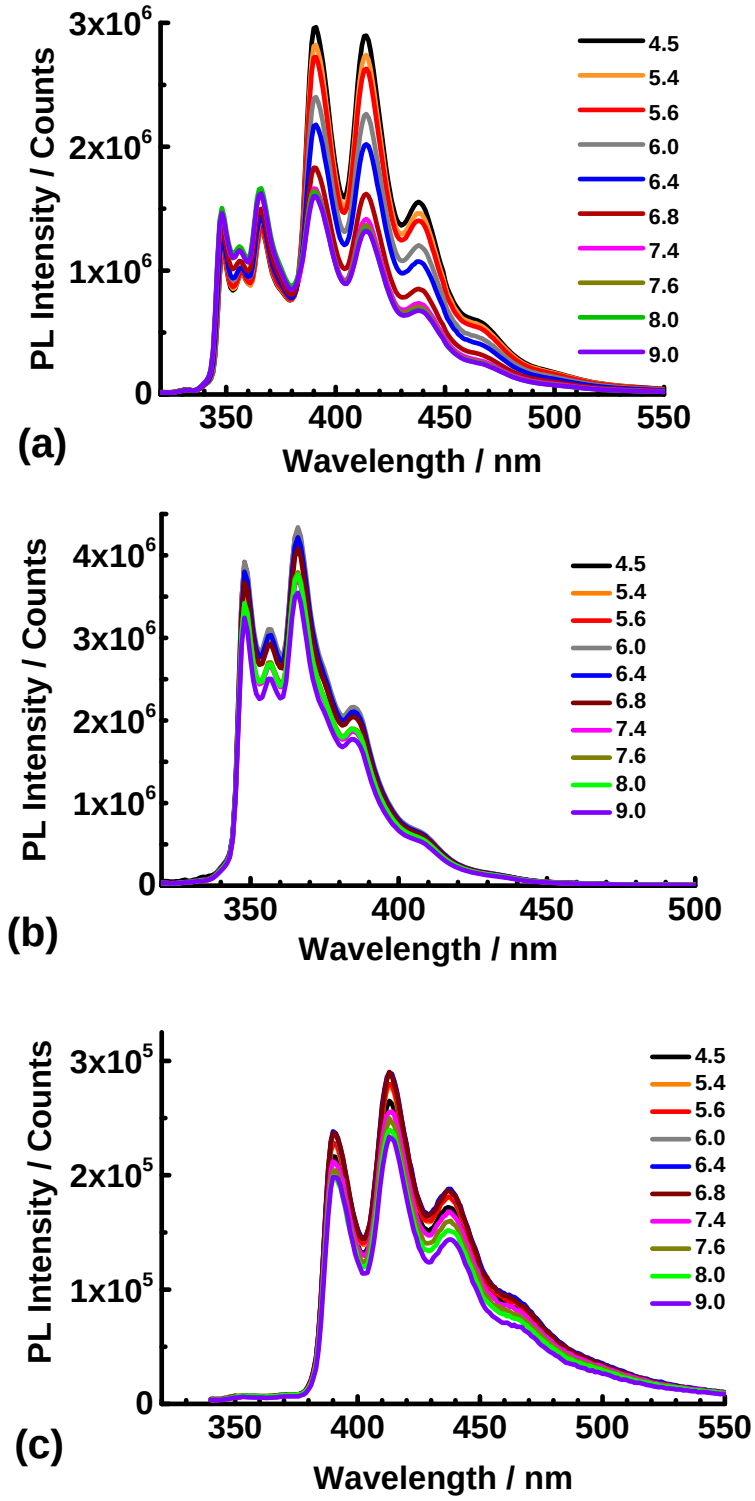

Figure S7. PL spectra for (a) $NG_{Ph/An}$, (b) NG_{Ph} and NG_{An} dispersions measured using a range of pH values (shown in the legends). The particle concentrations were 0.03 wt.%.

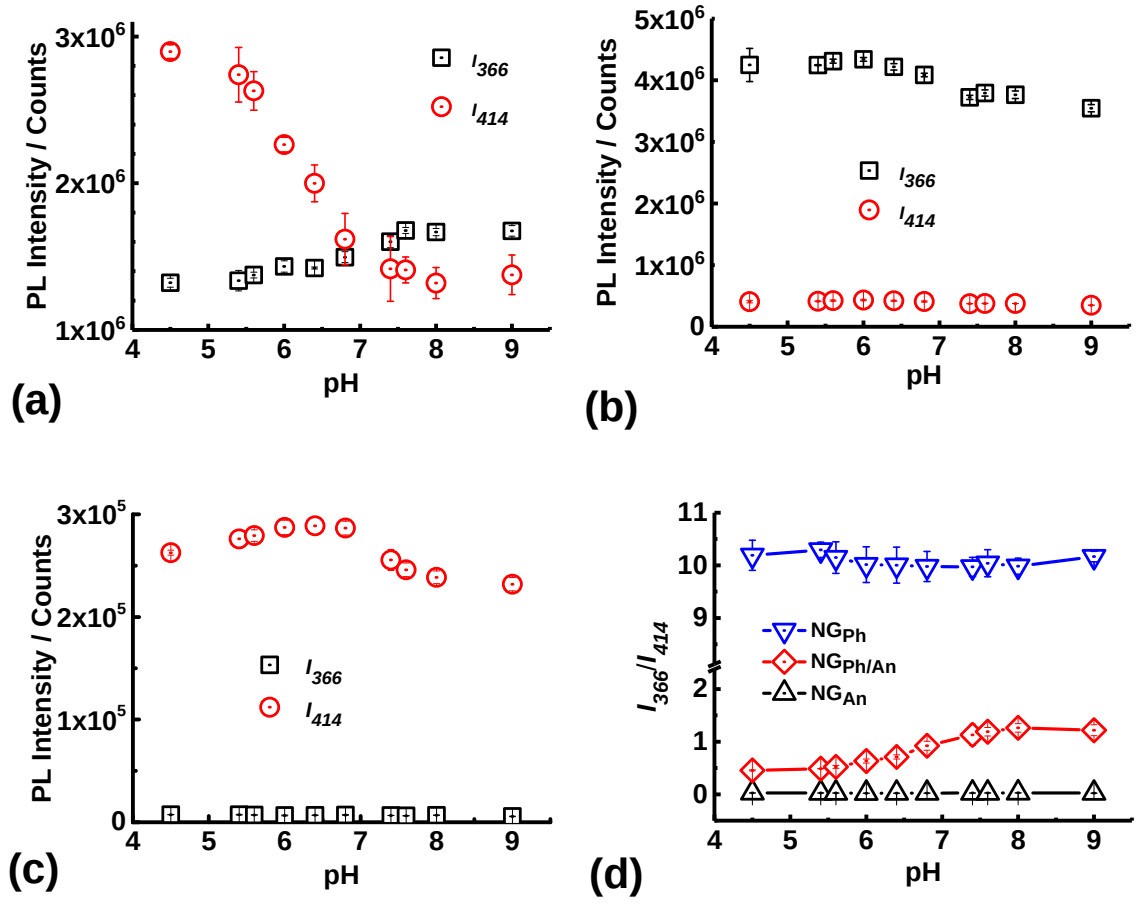

Figure S8 Variation of PL intensities measured at 366 and 414 nm for (a) $NG_{Ph/An}$, (b) NG_{Ph} and (c) NG_{An} dispersions. These data were taken from the respective spectra shown in Fig. S7. (d) shows the variation of I_{366}/I_{414} with pH for each dispersion. In some cases the error bars are smaller than the symbols.

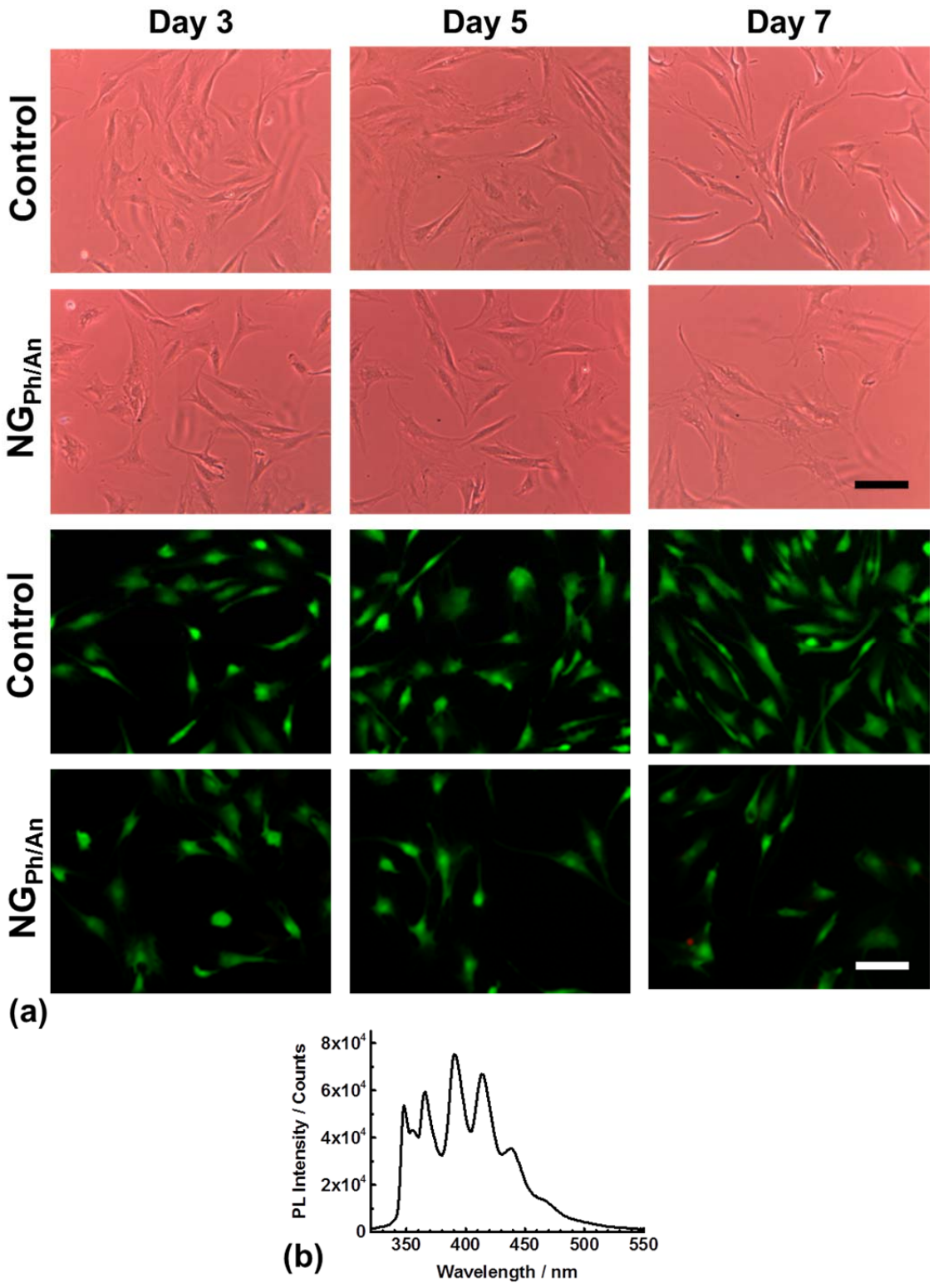

Figure S9. (a) Cell challenge data for human nucleus pulposus (NP) cells in the presence of a $NG_{Ph/An}$ dispersion (10^{-3} wt.%). Cell morphology images are shown (top two rows). Live/Dead assay images (bottom two rows) were obtained using a fluorescence microscope. (b) shows a PL spectrum for a $NG_{Ph/An}$ dispersion in PBS at the same particle concentration as used for (a). The scale bars apply to all images and represent 100 μm.

NRET efficiency calculation

The non-resonance energy transfer (NRET) efficiency was calculated using the intensities from the PL spectra measured for dispersed $NG_{Ph/An}$ particles (Figure S7a) and those obtained for NG_{Ph} (Figure S7b) using[2,8]

$$E = 1 - \frac{I_{D(NG_{Ph/An})}}{I_{D(NG_{Ph})}} = \frac{R_o^6}{R_o^6 + r^6} \qquad \text{(S3)}$$

where $I_{DA(\mathrm{NGPh/An})}$, $I_{D(\mathrm{NGPh})}$, R_o and r are the PL intensity of the donor signal (366 nm) for the $NG_{Ph/An}$ particles, donor intensity for the NG_{Ph} particles, Förster distance (2.3 nm[9]) and donor-acceptor distance, respectively. The Förster distance is the distance between the donor (Ph) and acceptor (An) for which the probability of the donor transferring its energy to the acceptor by dipolar resonance is equal to that of this energy being lost by fluorescence emission[9]. The R_o value is dependent on a number of values including the refractive index of the intervening medium. In accordance with earlier work for related microgel particles[2] we use the R_o value reported by Perez et al[9]. The values for $I_{DA(\mathrm{NGPh/An})}$ and $I_{D(\mathrm{NGPh})}$ were corrected[10] using the fluorophore concentrations in the $NG_{Ph/An}$ and NG_{Ph} particles (Table S2).

Additional core-shell $NG_{Ph/An}$ discussion

In addition to the data shown in Figure 1c support for a core-shell $NG_{Ph/An}$ structure comes from the pH-dependent electrophoretic mobility data (Figure S5). Such data are most sensitive to the outer surface of the swollen particles[11]. The present data show a rapid increase in the magnitude of the mobility at pH values greater than 5.5 which is followed by a more gradual increase at higher pH values. This behaviour would be generally expected from shell swelling followed by core swelling[11]. Accordingly, we propose that the shell of $NG_{Ph/An}$ particles had a lower local pK_a than the core. This explanation is consistent with the DLS data (Figure 1a) which showed that initial swelling occurred at pH values significantly below the apparent pK_a value for the particles (7.7, Table S2).

An interesting question concerns the homogeneity of the distribution of the dyes throughout the particles. The structures of Ph and An are similar (Scheme S1b) and so it is reasonable to expect that they had similar distributions within the $NG_{Ph/An}$ particles. Both dyes were less soluble than the structural monomers used to prepare $NG_{Ph/An}$ (Scheme S1a). One may expect that these dyes would have a higher concentration closer to the core than the shell of the particles on the basis of free-energy considerations[12]. However, a crosslinking monomer (EGMDA) was also used which can complicate the structure by preventing equilibrium structures from being achieved[13]. The data available (Fig. 1c) provided strong evidence that the dyes were present in both the core and shell of the particles and so they are proposed to have had a nominally uniform distribution.

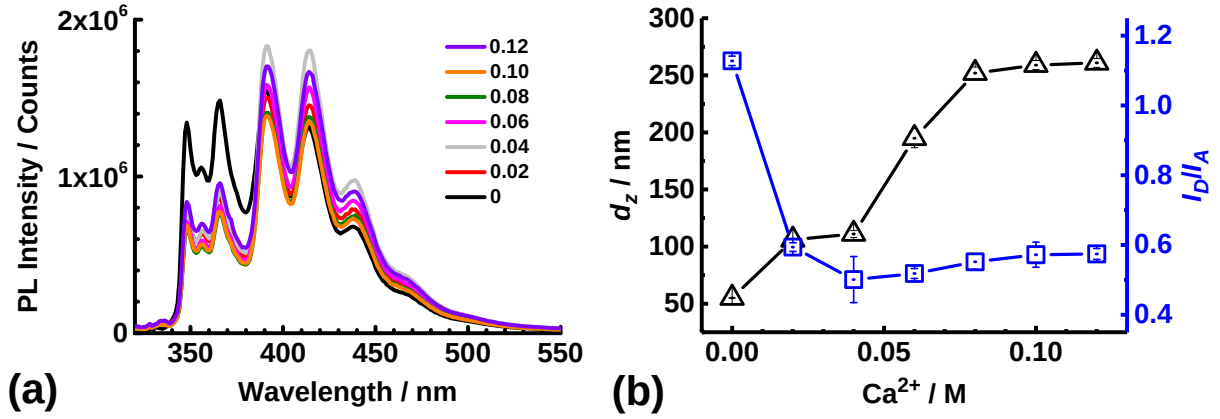

Figure S10. (a) PL spectra for $NG_{Ph/An}$ dispersions (pH 9.0) measured using different Ca^{2+} concentrations (shown in the legend in M). (b) Variation of d_z and I_D/I_A with Ca^{2+} concentration. The increase in d_z is due to aggregation.

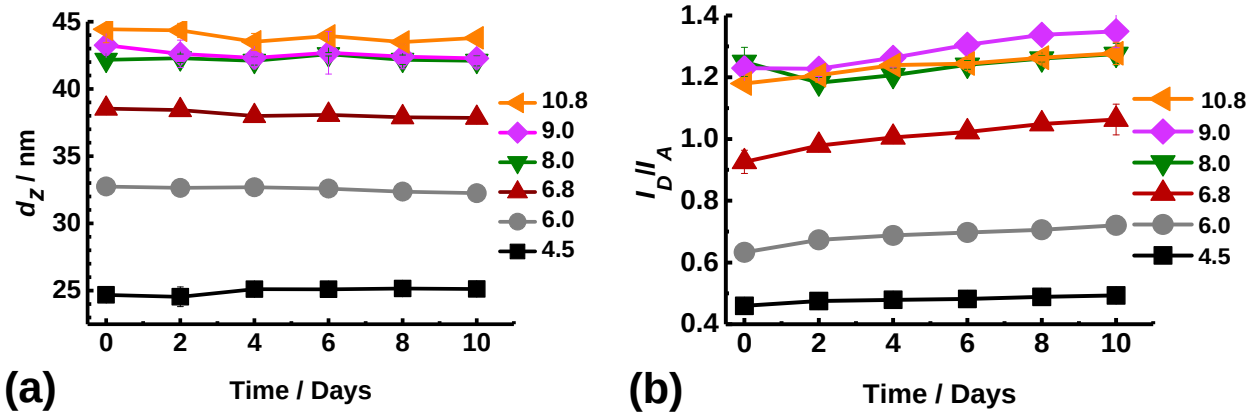

Figure S11. Variation of (a) d_z and (b) I_D/I_A for $NG_{Ph/An}$ with time measured at a range of pH values (shown). Whilst there was some drift in both the d_z values and I_D/I_A values the average change relative to the respective initial values was less than 10% over ten days.

DX NG hydrogel formation by covalently interlinking of NG particles

The pH-responsive hydrogels studied in this work were constructed from the NG particles (depicted in Scheme S1c). Following our earlier work[14] the pH of the concentrated dispersion was increased to greater than the pK_a to ensure that a physical gel formed. The NGs were subsequently covalently interlinked by free-radical coupling at 37 ^{o}C. This process transformed a shear-thinning physical gel into a covalently interlinked hydrogel. Figure S12 shows an image of DX NG(NG$_{Ph/An}$)$_{0.10}$ obtained using ambient light.

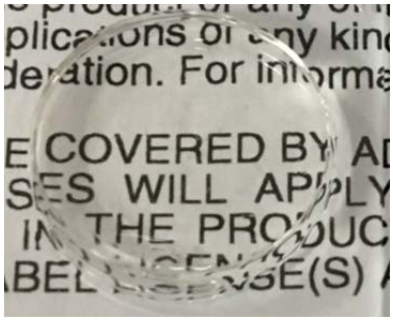

Figure S12 Image of as-made transparent DX NG(NG$_{Ph/An}$)$_{0.10}$ hydrogel obtained using visible light. The disc diameter was 15 mm and the thickness was 1.0 mm.

Comment about the use of non-vinyl functionalized $NG_{Ph/An}$ as reporter particles for gels

Our approach was not to vinyl functionalize the $NG_{Ph/An}$ particles in order to simplify their preparation and use. In addition, we hypothesized that these reporter particles would be effectively locked in place by the surrounding gel matrices and thereby provide sensitive reporting of the internal gel environment. When the DX NG/$NG_{Ph/An}$ gel was used (Scheme 1b) the $NG_{Ph/An}$ particles should have been locked in covalently interlinked NG cages. In the case of the PAAm-MBAAm($NG_{Ph/An}$) and PAAm-LAP($NG_{Ph/An}$) gels (AAm is acrylamide) there was expected to have been some inter-penetration of the NGs with PAAM chains which should have locked the $NG_{Ph/An}$ particles in place. Whilst these occurrences are consistent with the data presented (and are benefits) we cannot be certain that the $NG_{Ph/An}$ particles were intimately connected (and locked in place) within the gel networks discussed above. If incomplete connection of the nanoprobe particles with the network occurred, then a drawback might be that stress/strain transfer was not completely representative of the gel network that was being probed.

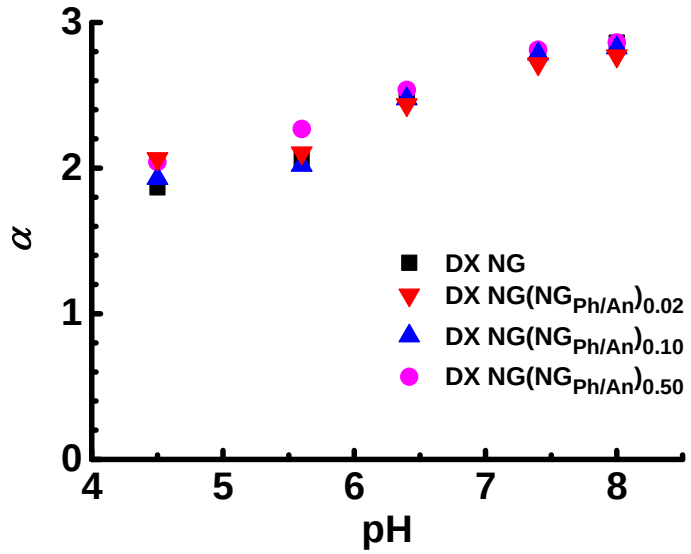

Figure S13. Variation of the average linear swelling ratio with pH for DX NG, DX NG($NG_{Ph/An}$)$_{0.02}$, DX NG($NG_{Ph/An}$)$_{0.10}$ and DX NG($NG_{Ph/An}$)$_{0.50}$ gels. There was no significant difference between the α values at each pH.

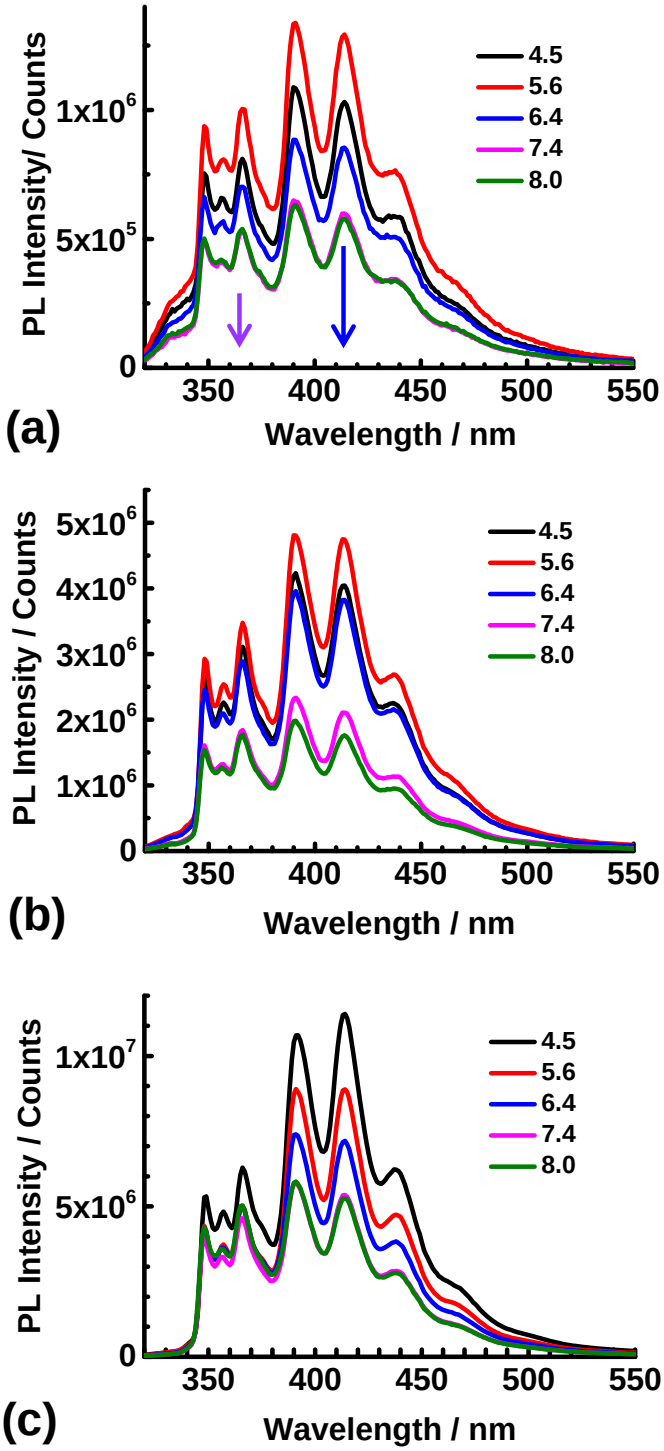

Figure S14 PL spectra for DX NG(NG$_{Ph/An}$)$_x$ gels containing NG$_{Ph/An}$ concentrations of (a) 0.02, (b) 0.10 and (c) 0.50%, respectively. The arrows in (a) show the direction of increasing pH.

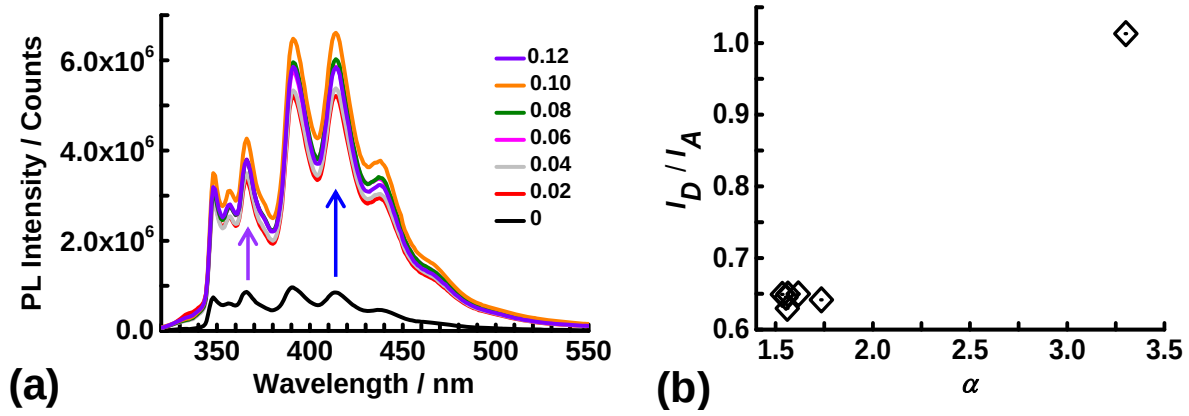

Figure S15. (a) PL spectra for DX NG(NG$_{Ph/An}$)$_{0.10}$ gel in the presence of different concentrations of $CaCl_2$ (shown in M). The arrows show the direction of increasing $CaCl_2$ concentration. (b) Variation of I_D/I_A with α. The pH was 8.9.

Using fluorescence to simultaneously study pH-triggered swelling and solute release

The pH-triggered release of RBITC from a DX NG gel (DX NG($NG_{Ph/An}$)$_{0.10}$) was monitored using fluorescence. Firstly, a calibration curve was constructed for RBITC (Figure S16a). RBITC-loaded gel samples were immersed in different buffer solutions and the supernatant analysed after 1 day and the concentration determined from application of the Beer-Lambert law. The concentrations of RBITC in the supernatant enabled the % release to be calculated (See Figure S16e). The I_D/I_A ratio measured for these systems were higher than expected when compared to the $NG_{Ph/An}$ dispersions (Figure 1a) and RBITC-free gel (Figure 2a). This effect is likely due to absorption of some of the donor emission by RBITC, which decreased the energy transfer to the acceptor. The wavelength range where absorption of the donor emission is proposed to have occurred is shown by the arrows in Figure S16a.

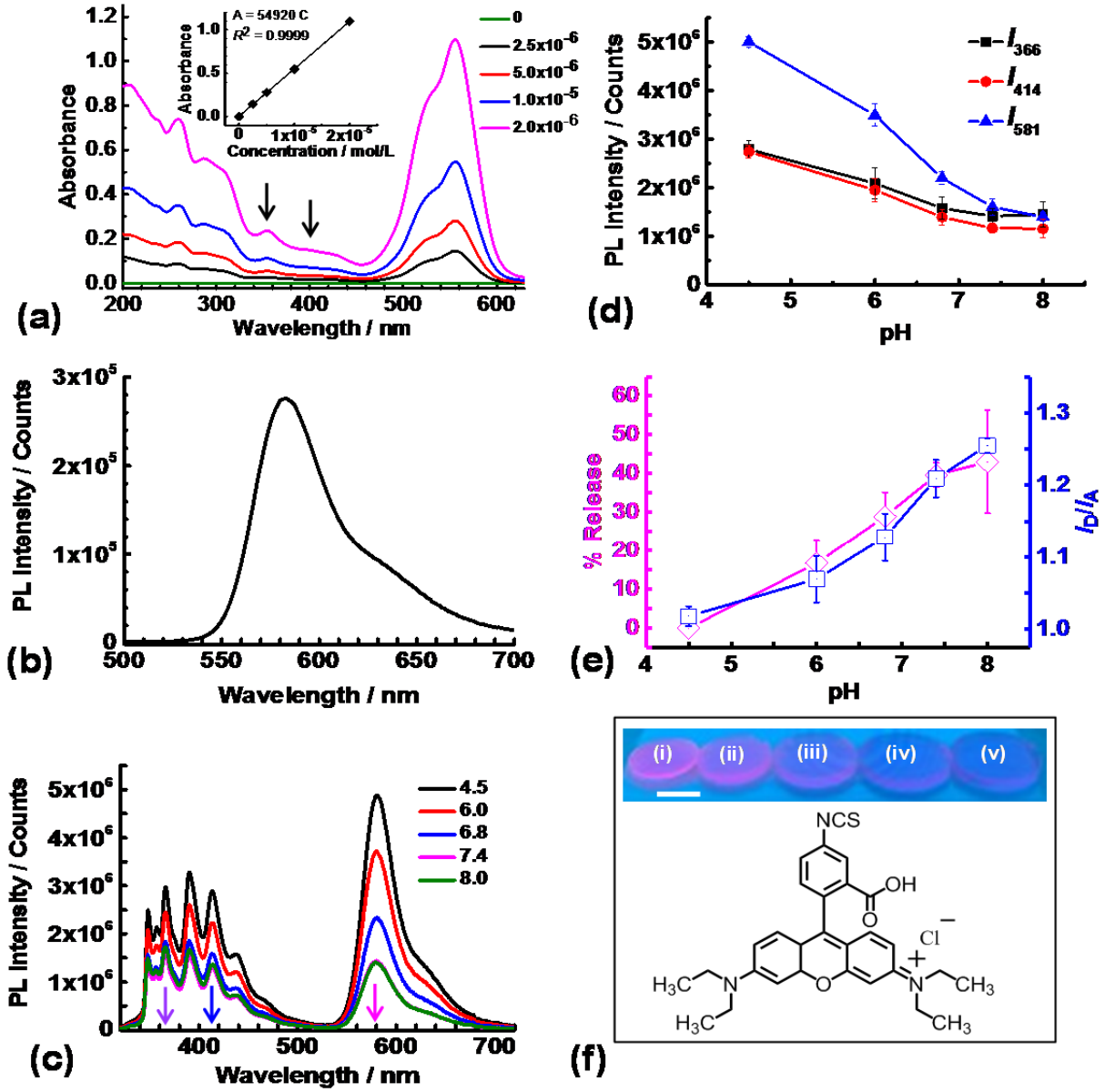

Figure S16. (a) UV-visible spectra and calibration graph (using absorbance at λ = 555 nm) for different concentrations of RBITC. The arrows show the range over which fluorescence from the $NG_{Ph/An}$ particles occurs (see text above). (b) PL spectra for RBITC with a concentration of 0.02 mM. (c) PL spectra for DX NG$(NG_{Ph/An})_{0.10}$ containing RBITC at various pH values. The arrows show the direction of increasing pH. (d) PL intensities at selected wavelengths against pH. (e) Variation of % RBITC release and I_D/I_A with pH. (f) Gel images (i - v) at pH 4.5, 6.0, 6.8, 7.4, 8.0 obtained using UV light (λ = 254 nm). The structure of RBITC is also shown.

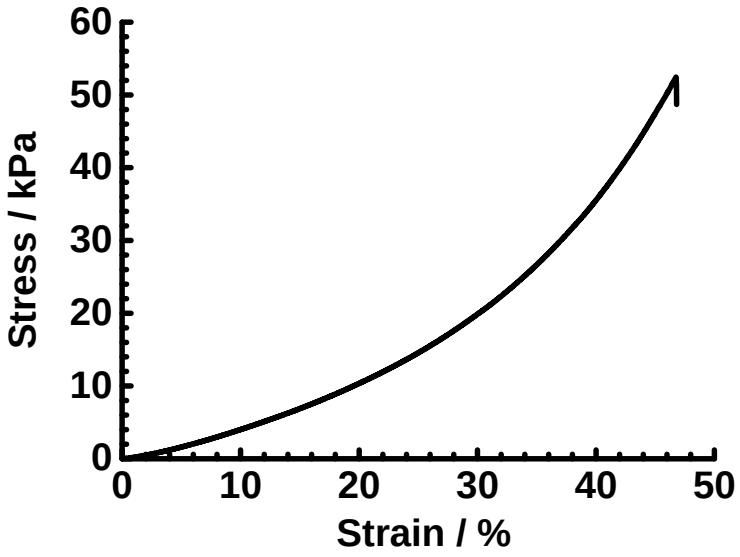

Figure S17. Uniaxial stress-strain data for DX NG($NG_{Ph/An}$)$_{0.10}$.

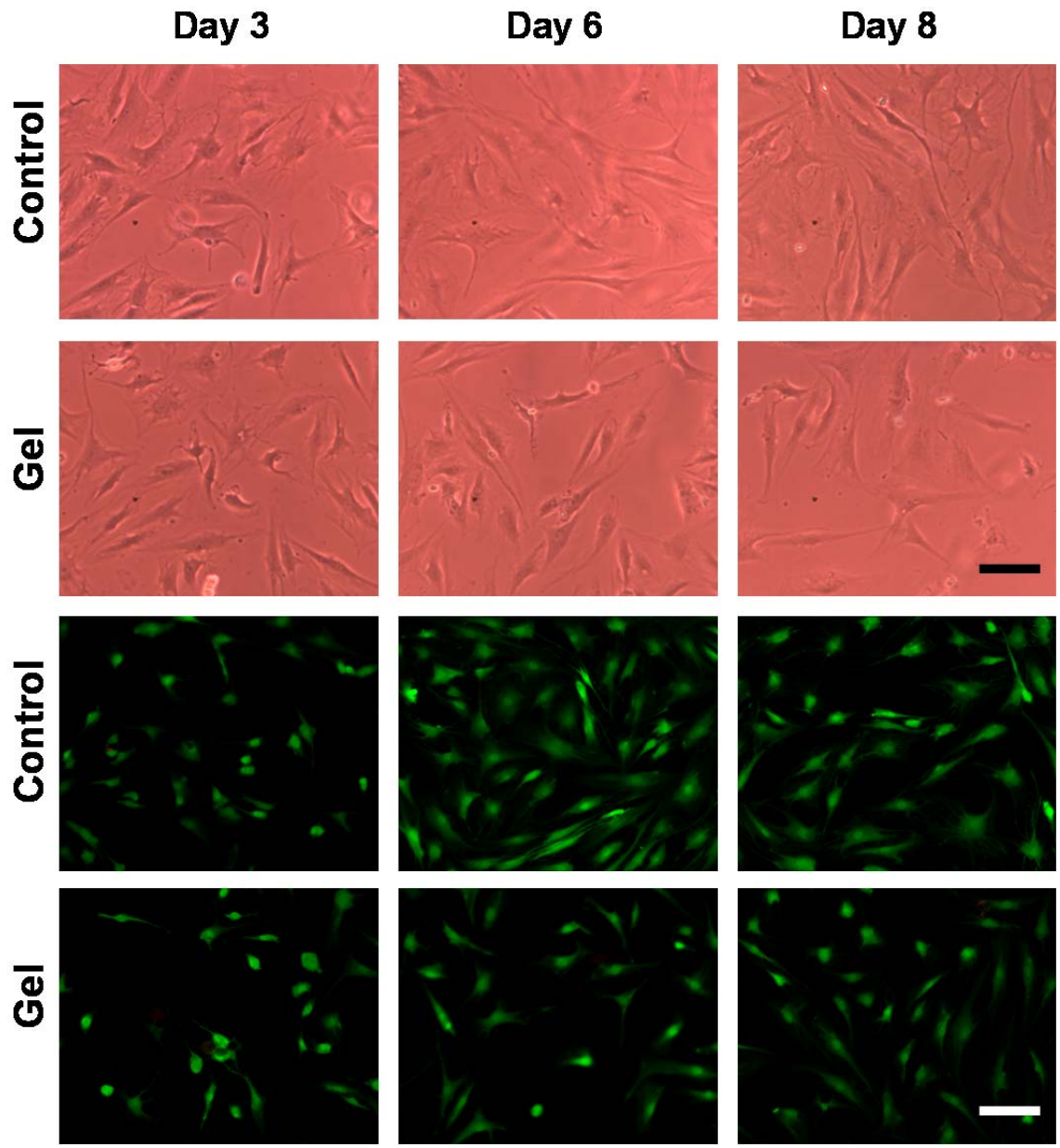

Figure S18. Cell challenge data for human nucleus pulposus (NP) of cells in the presence of DX NG/$(NG_{Ph/An})_{0.10}$ gel. The cells were in contact with the gel. Cell morphology images were obtained using an optical microscope (top two rows). Live/Dead assay images were obtained using a fluorescence microscope (bottom two rows). The scale bar applies to all images and is 100 μm.

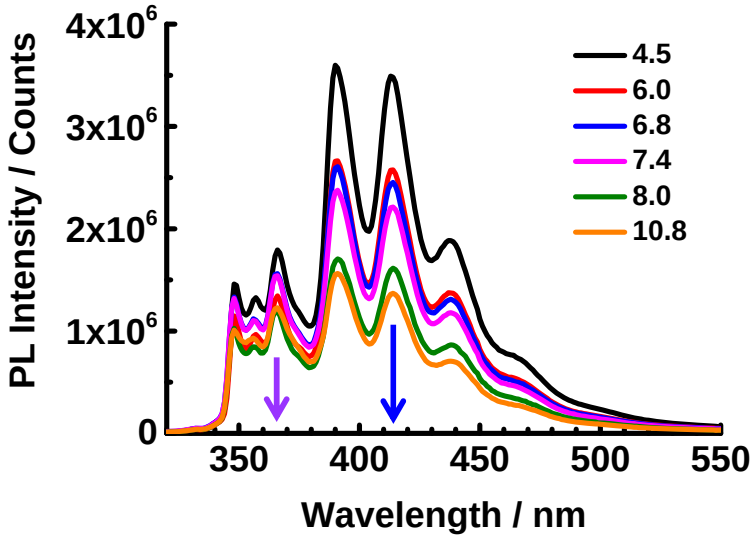

Figure S19. Effect of pH on PL spectra for PAAm-MBAAm($NG_{Ph/An}$)$_{0.10}$ gel. The arrows show the direction of increasing pH. The pH values are shown in the legend.

Figure S20. Digital photographs of PAAm-MBAAm($NG_{Ph/An}$)$_{0.10}$ gels containing universal indicator. The pH values were from left to right: 4.5, 6.0, 6.8, 7.4, 8.0, and 10.8. The solutions of indicator at the respective pH values are shown immediately above each gel.

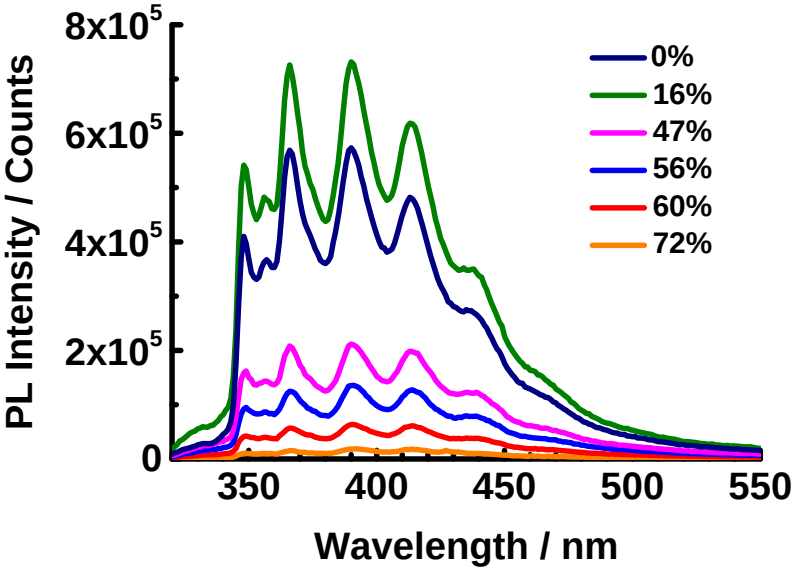

Figure S21. Effect of compressive strain on the PL spectra for PAAm-LAP($NG_{Ph/An}$)$_{0.03}$ gel.

Tables

Table S1 Materials used to prepare the nanogels

Nanogel	MMA / wt.%[a]	MAA / wt.%[a]	EGDMA / wt.%[a]	SDS / wt.%[b]	Ph / wt.%[a]	An / wt.%[a]	APS / wt.%[b]	Monomer mass / g[c]	Water / g
$NG_{Ph/An}$	77.5	19.3	1.66	0.51	0.80	0.75	0.050	1.66	19.6
Precursor[d]	79.3	18.9	1.89	0.50	-	-	0.070	106.0	480.0
NG_{Ph}	77.5	19.4	1.66	0.51	1.45	-	0.050	1.65	19.6
NG_{An}	77.4	19.3	1.66	0.51	-	1.68	0.050	1.66	19.6

[a] With respect to monomer. [b] Dissolved in water phase. [c]Total mass of all monomers added.

[d] Nanogel precursor used to prepare the GMA-functionalized NG (Scheme S1a).

Table S2 Composition and properties of the nanogels

Nanogel	MAA[a]/ mol%	GMA / mol%	pK_a[b]	Ph [c]/ mol %	An [c] / mol%	d_{TEM} [d] /nm	μ / x 10^{-8} m^2 /Vs[e] (pH 4.5)	d_z / nm (pH 4.5)	d_z / nm (pH 10)
$NG_{Ph/An}$	20.4	-	7.7	0.42	0.59	16 ± 3	-1.1 ± 0.2	24	44
NG	25.1	6.0	6.9	-	-	17 ± 4	-1.5 ± 0.1	30	70
NG_{Ph}	17.2	-	7.3	0.68	-	27 ± 8	-1.2 ± 0.1	35	58
NG_{An}	17.5	-	7.7	-	1.37	17 ± 4	-1.3 ± 0.1	25	43

[a] Calculated from potentiometric titration data shown in Figure S1. [b] Apparent pK_a values were obtained from data (Figure S1). [c] Determined from UV-visible spectroscopy data using the Beer-Lambert law (Figure S2). [d] Number-average diameters determined from TEM images. [e] Electrophoretic mobility.

Table S3 Composition and properties for the gels studied

Hydrogel	**$NG_{Ph/An}$ (%)**	**ϕ_p / %**[a]	**Modulus / kPa**	**Strain at break / %**	**Stress at break / kPa**
DX $NG(NG_{Ph/An})_{0.10}$	0.10	13.0 ± 0.1	19.1 ± 0.1	46.8 ± 0.4	52.5 ± 4.5
PAAm-$MBAAm(NG_{Ph/An})_{0.10}$	0.10	5.9 ± 0.6	3.0 ± 0.3	82.8 ± 1.8	21.3 ± 5.6
PAAm-$LAP(NG_{Ph/An})_{0.03}$	0.03	12.8 ± 0.2	2.5 ± 1.1	> 90% [b]	> 86 [b]

[a] Measured polymer volume fraction in the as-prepared state (Vol. %). [b] Gel did not break at maximum strain used for these measurements, which was 90%.

References

(1) Milani, A. H.; Saunders, J. M.; Nguyen, N. T.; Ratcliffe, L. P. D.; Adlam, D. J.; Freemont, A. J.; Hoyland, J. A.; Armes, S. P.; Saunders, B. R., Synthesis of polyacid nanogels: pH-responsive sub-100 nm particles for functionalisation and fluorescent hydrogel assembly, *Soft Matter* **2017**, *13*, 1554-1560.

(2) Gan, D. J.; Lyon, L. A., Interfacial nonradiative energy transfer in responsive core-shell hydrogel nanoparticles, *J Am Chem Soc* **2001**, *123*, 8203-8209.

(3) Pelah, A.; Seemann, R.; Jovin, T. M., Reversible Cell Deformation by a Polymeric Actuator, *J Am Chem Soc* **2007**, *129*, 468-469.

(4) Xiong, L. J.; Hu, X. B.; Liu, X. X.; Tong, Z., Network chain density and relaxation of in situ synthesized polyacrylamide/hectorite clay nanocomposite hydrogels with ultrahigh tensibility, *Polymer* **2008**, *49*, 5064-5071.

(5) Zhu, Y. X.; Wei, Z. W.; Pan, M.; Wang, H. P.; Zhang, J. Y.; Su, C. Y., A new TPE-based tetrapodal ligand and its Ln(III) complexes: multi-stimuli responsive AIE (aggregation-induced emission)/ILCT(intraligand charge transfer)-bifunctional photoluminescence and NIR emission sensitization, *Dalton Trans.* **2016**, *45*, 943-950.

(6) Karadağ, E.; Saraydın, D.; Güven, O., Radiation Induced Superabsorbent Hydrogels. Acrylamide/Itaconic Acid Copolymers, *Macromol. Mater. Eng.* **2001**, *286*, 34-42.

(7) Everett, D. H. *Basic principles of colloid science*; Royal Society of Chemistry: London, 1988.

(8) Lackowicz, J. R., *Principles of fluorescence spectroscopy, Springer, NY* **2006**.

(9) Pérez, E.; Lang, J., An Inversion Method for the Determination of the Internal Structure of Latex Particles from Fluorescence Nonradiative Energy Transfer Experiment, *J. Phys. Chem. B.* **1999**, *103*, 2072-2084.

(10) Parker, C. A.; Rees, W. T., Correction of Fluorescence Spectra and Measurement of Fluorescence Quantum Efficiency, *Analyst* **1960**, *85*, 587-600.

(11) Daly, E.; Saunders, B. R., Temperature-dependent electrophoretic mobility and hydrodynamic

radius measurements of poly(N-isopropylacrylamide) microgel particles: structural insights, *Phys. Chem. Chem. Phys.* **2000**, *2*, 3187-3193.

(12) Stubbs, J.; Tsavalas, J.; Carrier, R.; Sundberg, D., The Structural Evolution of Composite Latex Particles During Starve-Fed Emulsion Polymerization: Modeling and Experiments for Kinetically Frozen Morphologies, *Macromol. React. Eng.* **2010**, *4*, 424-431.

(13) Sundberg, D. C.; Durant, Y. G., Latex Particle Morphology, Fundamental Aspects: A Review, *Polym. React. Eng.* **2003**, *11*, 379-432.

(14) Milani, A. H.; Fielding, L. A.; Greensmith, P.; Saunders, B. R.; Adlam, D. J.; Freemont, A. J.; Hoyland, J. A.; Hodson, N. W.; Elsawy, M. A.; Miller, A. F.; Ratcliffe, L. P. D.; Mykhaylyk, O. O.; Armes, S. P., Anisotropic pH-Responsive Hydrogels Containing Soft or Hard Rod-Like Particles Assembled Using Low Shear, *Chem. Mater.* **2017**, *29*, 3100-3110.